Available online at www.sciencedirect.com
SCIENCE DIRECT®
PERGAMON
International Journal of Heat and Mass Transfer 46 (2003) 3291–3297
International Journal of HEAT and MASS TRANSFER
www.elsevier.com/locate/ijhmt

Annular synthetic jet used for impinging flow mass-transfer

Zdeněk Trávníček [a,*], Václav Tesař [b]

[a] Institute of Thermomechanics, Academy of Sciences of the Czech Republic, Dolejškova 5, Prague 8 182 00, Czech Republic

[b] The University of Sheffield, Mappin Street, Sheffield S1 3JD, United Kingdom on leave from CVUT Czech Technical University, Prague, Czech Republic

Received 16 October 2002

Abstract

An annular synthetic jet was investigated experimentally, both with and without an opposing impingement wall. The experiments involved smoke visualization and mass transfer measurement on the wall by means of naphthalene sublimation technique. Two qualitatively different flow field patterns were identified, depending upon the driving amplitude level. With small amplitudes, vortical puffs maintain their identity for a relatively long time. If the amplitudes are large, breakdown and coalescence of the vortical train is much faster. Also the resultant mass transfer to the impingement wall is then much higher. Furthermore, a fundamental change of the whole flow field was observed at the high end of the investigated frequency range, associated with radical reduction of the size of the recirculation bubble.

1. Introduction

Due to the nonlinearity of the inertial term in the governing equation, pulsating flows usually exhibit a marked asymmetry, which is variously known as fluidic rectification, aerodynamic streaming, or (at high frequencies) acoustic streaming. A driving action with fully symmetric cycles (such as e.g. purely sinusoidal driving pressure without a time-mean component) may result in a flow exhibiting a pronounced unidirectional motion. In the case of an alternating flow out from and into a nozzle, this asymmetry of the response leads to a quite different character of the inflow and outflow phases. The "puff" accelerated during the flow from the nozzle, together with the entrained surrounding fluid, is directed away from the nozzle and this is not compensated by an equally strong return inflow during the suction phase. Instead, fluid is "inhaled" into the nozzle from the stagnant sideways locations. As a result, the time-mean flow comes from these sideways locations and is directed away from the nozzle. The overall time mean motion is thus very similar to that generated by a steady jet. The effect was first observed in the thirties as the so called "loudspeaker wind" in the first radio receivers with a loudspeaker. The interest was initially turned towards this phenomenon in view of possible application of the rectification capability in valveless reciprocating pumps and blowers [1,2]. One of the present authors was among the first investigators who studied the phenomenon and found and important governing laws [3–5].

Recently, such *synthetic jets* (in the sense of being synthetised from the surrounding fluid) were proposed (Glezer et al. [6], Smith and Glezer [7], Glezer and Amitay [8], Tesař and Zhong [9]) for air jet vectoring (Smith and Glezer [10]), and for active control of turbulence or flow separation both in internal (Benchiekh et al. [11]) as well as external aerodynamics (Glezer et al. [6]; Amitay and Glezer [12], Tensi et al. [13]). The basic advantage is the absence of supply piping for fluid delivery to each actuator. The attention is usually limited to the basic round or slot nozzle geometry.

Synthetic jets may be potentially attractive for impinging jet cooling and heating. Their highly agitated flow fields can achieve high heat transfer rates. This, together with the advantage of no supply ducting (which

* Corresponding author. Tel.: +420-2-6605-3302; fax: +420-2-8658-4695.
E-mail address: tr@it.cas.cz (Z. Trávníček).

0017-9310/03/$ - see front matter © 2003 Elsevier Science Ltd. All rights reserved.
doi:10.1016/S0017-9310(03)00119-4

Nomenclature

D_i	inner diameter of annular nozzle, $D_i = 38$ mm	f	excitation frequency
D_o	outer diameter of annular nozzle, $D_o = 40$ mm	h_m	local mass transfer coefficient, Eq. (1)
D_{naph}	mass diffusion coefficient of naphthalene vapor in air [25]	H	nozzle-to-wall spacing
		Sh	Sherwood number, $h_m D_o/D_{naph}$

otherwise tends to occupy too much of the valuable space in miniature devices) makes the impinging synthetic jets an extremely promising alternative for applications such as cooling of electronic components [15]. One of the first investigations of this subject was briefly described by Yassour et al. [14]. As usual, they experimented with simple round nozzles, similarly as did Glezer and Vukasinovic [16].

Heat and mass transfer under impinging jets have been widely studied. Main results have been collected in several reviews, e.g., one of the first was published by Martin [17], and recent one has been presented by Garimella [18] (who, apart from having discussed his own results, shows 122 relevant references). Impinging jets issuing from an annular nozzle was investigated, e.g. [19,20], and present authors recently found some useful and attractive features of this geometry [21]. In particular, it was established that the wall transport phenomena of that this type of impinging flow may be increased by applied pulsation [22,23]. This is a marked advantage over simple round nozzle impinging jets, where improvements in the heat transfer efficiency are generally elusive—sometimes there is an increase (small), sometimes a decrease—see Herman [24]. It is therefore natural to use the same annular nozzle geometry also for investigations of *annular synthetic impinging jets*. To the best authors' knowledge, this flow configuration was not suggested in available literature until now.

2. Experimental facilities and techniques

Fig. 1 shows a schematic view on the used annular nozzle. The nozzle is situated vertically and its inner and outer exit diameters are $D_i = 38.0$ mm and $D_o = 40.0$ mm, respectively. The flow is generated by the loudspeaker of 100 mm diameter (TESLA ARN 100 10/4), fed by a sinusoidal current. For study of the jet impingement, a plane wall is inserted opposite to the nozzle exit, perpendicular to the nozzle axis. The wall for visualization is made out of plywood, and it is covered with a plastic black foil. The wall for mass transfer experiments is a naphthalene plate as described below. Experiments were performed in a test chamber (width

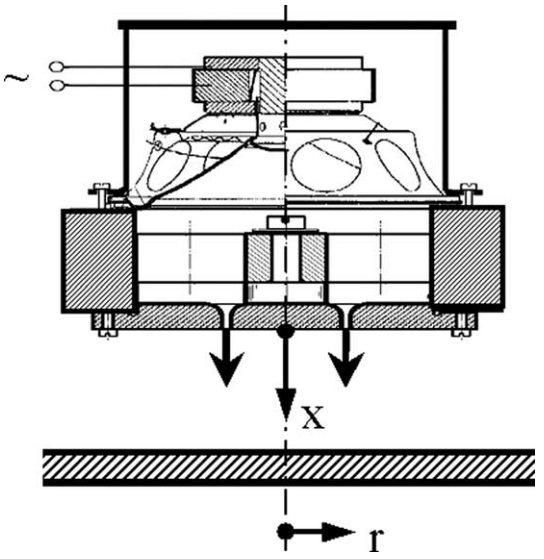

Fig. 1. Annular nozzle with an acoustic excitation.

1.3 m × depth 0.8 m × height 1.8 m), well ventilated outside the laboratory (because of naphthalene experiments). Thick glass-fiber curtain around the chamber (except observation window) effectively avoided direct reflection of the sound into the flow field.

Sound pressure level (SPL) was measured by means of the sound level meter QUEST 210 (frequency weighting networks A), with its microphone (dia. 13.5 mm) located perpendicularly to the nozzle axis in the point of $x = 10$ mm, $r = 40$ mm. The "A" weighting response, used by the device, emulates the low level response of the human ear. For comparison purpose the measured values SPL were transformed into the more physical "C" weighting response (SPL_C).

A smoke-wire technique was used for the visualization of air jet downstream the nozzle. Smoke-wire was made from three resistance wires with 0.1 mm in diameter, which were uniformly twisted together. It was coated by paraffin oil before each test, and heated by DC current Joule effect. Contrasting white streaklines on black background were observed and photographed, illuminated alternatively by one of the three light sources:

continuous bulb light, flashlight, and stroboscope light synchronized with excitation source. The time-mean flow field pattern (pathlines), instantaneous pattern (streaklines), and phase-locked streaklines were observed, respectively. Pictures were taken by a digital camera.

Local mass transfer was measured by evaluating naphthalene sublimation from the exposed wall [25]. The test surface is produced by casting naphtalene into a robust steel mold, with the active surface well polished and chromium-plated. The size of the exposed surface was 130 mm × 450 mm. Measurement of the depth of the surface depression due to sublimation was performed on the XY table as the difference between "Before Run" and "After Run" surface measurement. The measurement system consisted of eight depth gages connected to signal conditioners (linear variation differential transformers, TOMES Krupka, Czech Republic), stepping-motor driven positioner, a hardware unit for motor control, and PC computer equipped with I/O board (NATIONAL INSTRUMENTS, AT-MIO-16E-10). The depth gages were traversed across the naphthalene specimen at an equidistant spacing 10 mm. Typical total number of data points are 2400, each of these points comprises an average of 10 partial sampling. The local mass transfer coefficient is calculated from the sublimation depth Δx as

$$h_m = \frac{\rho_n R_n T_w \Delta x}{p_{sat} \Delta t} \quad (1)$$

where ρ_n is the density of solid naphthalene, ($\rho_n = 1175$ kg/m^3 at 20 °C), R_n is the gas constant of naphthalene ($R_n = 64.87$ J/(kg K)), T_w is the exposed surface absolute temperature (evaluated from the temperature of air jet, taking into account aerodynamic heating and sublimation of the wall; the wall temperature depression was typically 0.1–0.12 K below the measured air temperature), Δx is net local sublimation depth, p_{sat} is the saturated vapor pressure of naphthalene at the surface temperature, and Δt is the run duration. The extraneous sublimation due to natural convection (during the specimen manipulation and its surface measurement) has been evaluated by an auxiliary experiment, and is subtracted from the total sublimation depth; the resultant correction of the h_m-value was typically 0.0023 m/s. The maximum sublimation depth was 0.1 mm, the run duration time was 45–140 min.

Non-dimensional expression of mass transfer coefficient is the Sherwood number, $Sh = h_m D_o / D_{naph}$, where D_{naph} is the mass diffusion coefficient of naphthalene vapor in air, calculated for measured temperature and pressure [25].

Two thermistor probes, connected with THERM 2280-3, were used to measure air temperature, one located in ambient air, the other one inserted in the nozzle exit before each test run, to make sure that experiments are made after required temperature equalization. The temperature range was from 21.5 to 23.2 °C for all experiments.

Uncertainty analysis was performed according to Kline and McClintock's method [26] for single sample experiment. The uncertainty of the solid naphthalene density ρ_n, temperature T_w, sublimation depth Δx, duration of test run Δt, nozzle diameter D_o, saturated vapor pressure p_{sat}, and mass diffusion coefficient D_{naph} were estimated 1.1%, 0.06%, 4.3%, 0.5%, 0.1%, 3.77%, and 5.1%, respectively. The uncertainty of the mass transfer coefficient and the Sherwood number is within 6% and 9% in the entire range of measurements based on a 95% confidence level (±2 standard deviation).

3. Results and discussion

Two different level of the acoustic excitation were used, labeled here as "weak" and "strong"; the input electrical power into the loudspeaker was 0.16 and 4.0 W, respectively. The parameters of experiments discussed in this paper are shown on Table 1.

SPL and SPL_C, increases with decreasing nozzle-to-wall spacing, H, because of the reflection of the sound from the exposed wall.

The frequency dependence of the excitation amplitude at the same input power is caused by resonance in the settling chamber upstream from the nozzle, containing the loudspeaker (and the frequency dependence of the loudspeaker itself, which is insignificant). This is the common disadvantage—cf. e.g. Lepičovský et al. [27]—of this pulsation generation method.

Table 1
Parameters of experiments

Task	Excitation (electrical power, W)	Excitation frequency, f, Hz	Nozzle-to-wall spacing, H, mm	Sound pressure level	
				SPL, dB	SPL_C, dB
1	weak (0.16 W)	106.0	∞, 40, 20	66.0, 74.0, 82.3	83, 91, 99
2	strong (4.0 W)	106.0	∞, 40, 20	72.5, 86.0, 95.6	89, 103, 113
	strong (4.0 W)	155.0	∞, 40, 20	84.5, 104.8, 106.7	98, 105, 120
	strong (4.0 W)	263.0	∞, 40, 20	93.7, 116.0, 118.4	102, 125, 127
	strong (4.0 W)	692.0	∞, 40, 20	110.0, 128.6, 129.9	112, 130, 132

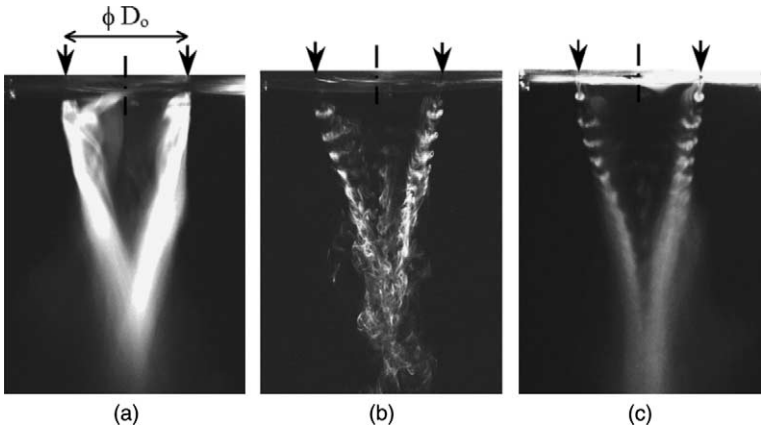

Fig. 2. Synthetic jet at "weak" excitation, frequency $f = 106$ Hz: (a) time-mean flow field—continuous exposure over a large number of cycles; (b) instantaneous streaklines—a single short exposure; (c) mean streaklines—multiple exposure (106 superimposed frames taken at instants phase-locked to the beginning of the excitation cycle).

3.1. Character of the flow—flow visualization

Fig. 2 presents visualised flow field of the synthetic jet without the impingement wall. The excitation was "weak" (0.16 W electrical input). The time-mean picture Fig. 2(a) provides and idea of the trajectories of motion of individual vortices formed at the nozzle exit, which are apparent in the instantaneous streaklines in Fig. 2(b). The trajectories come together and merge on the nozzle axis, at the location roughly $x \sim 2D_o$ from the nozzle, which corresponds to the re-attachment point of steady annular jets [21]. The individual vortices are distinguishable all the way from the nozzle up to a considerable streamwise distance (roughly $1.5D_o$ to $2D_o$), beyond which they break down. The details of the process are best seen in multiple exposure Fig. 2(c), which shows 106 superimposed frames, taken one after another at each cycle during 1 s, at zero phase shift with respect to the beginning of the excitation cycle. The picture shows the phase-locked emission lines, smoothing out the fluctuation deviations of individual cycles.

Somewhat surprisingly, the visualisation results for the otherwise same conditions of the annular synthetic jet (without impingement wall) differ considerably when the "strong" excitation (4.0 W electrical input) is applied, Fig. 3. The streaklines there (Fig. 3(b and c)) show clearly a single large toroidal vortex, located at about $x = 0.5D_o$ from the nozzle exit. Further downstream, the visualisation does not reveal any periodic structures - at least at the frequency equal to the excitation frequency $f = 106$ Hz and the vortices break down there.

3.2. Mass transfer experiments

Fig. 4 presents an example of results of the mass transfer measurement on the impinging wall. In this case

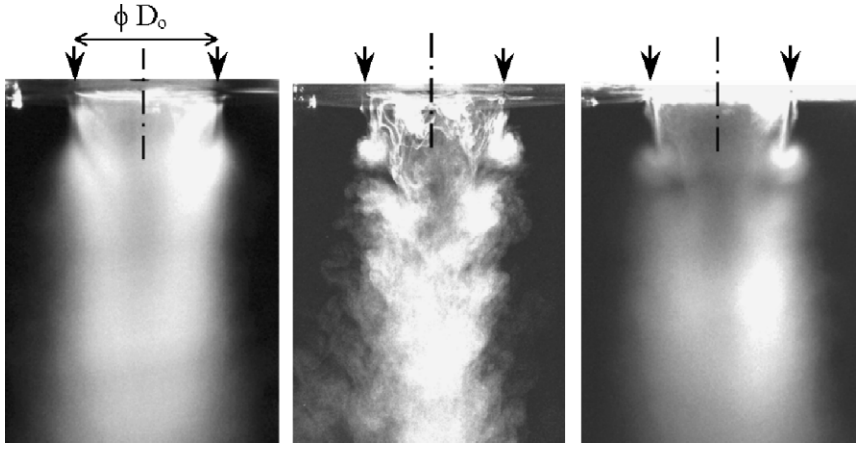

Fig. 3. Synthetic jet at "strong" excitation, the same frequency $f = 106$ Hz as in Fig. 2(a), (b), (c)—legends are the same as in Fig. 2.

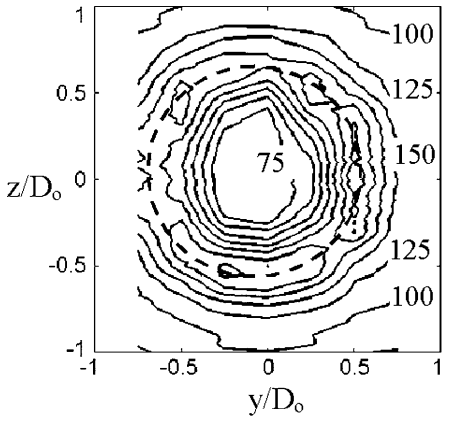

Fig. 4. Mass transfer onto wall exposed by "strong" excitation, $H = D_o/2$, $f = 106$ Hz. Steps between *Sh*-lines are 25.

it was the "strong" excitation case at frequency $f = 106$ Hz—the same as in the flow visualisations discussed above (Fig. 3). The impingement wall was placed at the distance $H = D_o/2$ below the nozzle exit. The lines plotted in Fig. 4 are lines of constant time-mean mass transfer, nondinmensionalised to the Sherwood number *Sh*. The highest values of the mass transfer coefficient are on the stagnation circle (broken line in Fig. 4) the diameter of which is $1.2D_o$, slightly larger than the outer diameter D_o of the nozzle exit.

The symmetric, nearly circular character of the lines in Fig. 4 gives an idea of the symmetry of the experiment. The small azimuthal variations are due to nozzle manufacturing tolerances and measurement errors rather than due to presence of any azimuthal structures. It should be noted that the flow field is quite near to an instability (Fig. 5(b) below) which tends to amplify the influence of even small errors of the setup, so that the shapes in Fig. 4 are a proof a careful adjustment.

The next Fig. 5(a) presents the mass transfer experiment results for the $H = D_o/2$ wall distance, same as that for Fig. 4. The difference between the two halves of the diagram gives an idea about the achievable symmetry of the flow field. The data for the lowest frequency, $f = 106$ Hz, show that in the "strong" case, as expected, the mass transfer intensity is considerably higher than the "weak" case.

At most of the frequencies in Fig. 5(a), the mass transfer maximum takes place on the stagnation circle, but there is also a lower local maximum on the nozzle axis. This is explained by the "*centripetal*" character [21] of the flow at the wall towards the axis, where there is a "reverse stagnation point" [20].

The Fig. 5(b) shows—plotted in an analogous manner to Fig. 5(a)—the mass transfer experiment results for the impingement wall placed at a distance from the nozzle twice as large. The first fact that should be noted is the higher value of the mass transfer coefficient in the "weak" jet case than in Fig. 5(a). The effect is remarkably large: quite contrary to what could be expected when the distance is increased, the *Sh* values are now nearly twice as high. The explanation we can offer is the wall at $H = 0.5D_o$ being (cf. Fig. 2) in the flow field of rather stable individual vortices. On the other hand, at $H = D_o$ being (cf. Fig. 2) the vortices already undergo a breakup before reaching to the wall, the flow there becoming turbulent. On the other hand, in the "strong" impinging synthetic jet cases, the vortices break up earlier so that there is little difference between the flow at this distance ($H = 0.5D_o$) and at $H = D_o$.

Another remarkable fact following from the comparison of Fig. 5(a) and Fig. 5(b) is the essential difference of the character for the highest tested excitation frequency, $f = 692$ Hz. It is evident that the stagnation circle for $H = D_o$ disappears and the flow field possesses the "*closed pattern*" [19] character. This is a remarkable fact an important finding: merely by increasing the excitation frequency from $f = 293$ Hz to $f = 692$ Hz in Fig. 5(b), the topology of the near-wall flow underwent an essential change in the topological character: the "*centripetal*" character (streamlines heading towards the central point, [21]) is reversed into the "*centrifugal*"

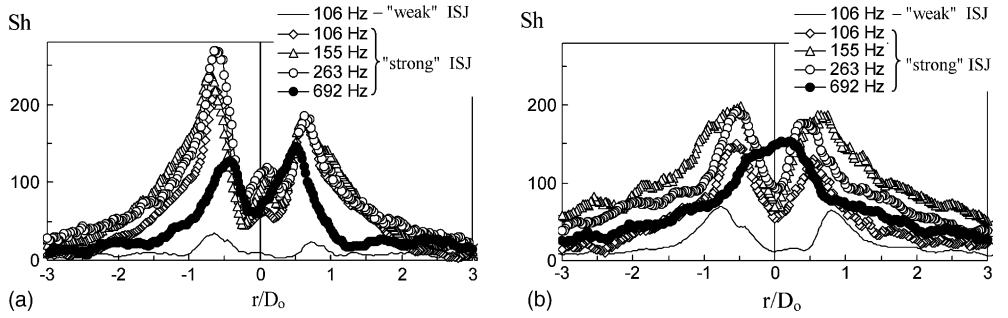

Fig. 5. Mass transfer results: radial distribution of Sherwood number on the impingement plate (a) $H = D_o/2$, (b) $H = D_o$.

character, with streamlines heading away from the centre. The change also results—because of the radial divergence and the consequently larger area covered by the high-intensity stagnation region at the lower frequencies—in a marked change of the magnitude of the overall mass (and, of course, also heat) transfer between the fluid and the wall.

This is a remarkable fact from a flow control point of view: it is possible to get two fundamentally different solutions of the flow field, defined by the same geometry, in response to a change in the generation frequencies. In fact, although we did not study in closer detail the range of the frequencies in which this transition takes place, we have already found in similar situation an alternative existence of the two flow fields even under the same conditions (the same geometry and even the same boundary conditions). These are very interesting problems associated with stability, bistability and hysteretic behaviour—see the paper by Trávníček and Křížek [28] (probably the first publication on the bistability an hysteresis of impinging jets in a reviewed journal at all), and [19,21].

4. Conclusions

Experimental investigations of the annular impinging synthetic jet by means of smoke wire visualisation and the wall mass transfer measurements discovered several mutually different types of the flow. Depending upon the amplitude of the generation (''weak'', ''strong''), two different types could be identified of the development of the synthetic jet. In the first case, the vortices generated by individual outflows (''puffs'') retain their identity for a considerable distance. In the other case, a rather rapid break-up of the vortices takes place. In most investigated cases, at low excitation frequencies, the flow field is dominated by a large recirculation bubble of a separated flow reaching up to the impingement wall. With the ''strong'' excitation at the highest excitation frequency, the character of the flow field is different, the bubble collapses into a relatively small bubble position right at the nozzle body wall. The transition is due to a spectacular instability.

Present experiments are an introduction into the studies of the annular impinging synthetic jets that seem to be very promising for applications in cooling thermally highly loaded surfaces, such as those of electronic components.

Acknowledgements

We gratefully acknowledge the support by the Grant Agency of the Czech Republic (projects no. 101/99/0059, 101/99/0060), and by the Grant Agency of the Academy of Sciences of the Czech Republic (project No. A1057001).

References

[1] V. Tesař, Pump or blower, in particular for transporting fluids difficult to pump (in Czech), Czechoslovak Certificate of Authorship No. 192 082 (1976).
[2] V. Tesař, Proc. Colloquium on Pneumatics and Hydraulics PNEU-HIDRO'81, Györ, Hungary, 57 (1981).
[3] V. Tesař, Law governing entrainment of surrounding fluid during alternating inflow into and outflow from an orifice (in Czech), Application PO 86-84, Patent Office, Prague (1984).
[4] V. Tesař, Fluidics Quarterly, Ann Arbor USA 14 (1982) 4.
[5] V. Tesař, Acta Polytechnica—Práce ČVUT v Praze II—1, 43 (1991).
[6] A. Glezer, M.G. Allen, D.J. Coe, B.L. Smith, M.A. Trautman, J.W. Wiltse, Synthetic Jet Actuators and Applications Thereof, US Patent No. 5758823 (1998).
[7] B.L. Smith, A. Glezer, Physics of Fluids 10 (1998) 2281.
[8] A. Glezer, M. Amitay, Annual Review of Fluid Mechanics 34 (2002) 503.
[9] V. Tesař, S. Zhong, Proc. fourth Pacific Int. Conf. on Aerospace Science and Technology PICAST 4, Kaohsiung, Taiwan ROC, 129 (2001).
[10] B.L. Smith, A. Glezer, J. Fluid, Mechanics 458 (2002) 1.
[11] M. Benchiekh, J-C. Bera, M. Michard, M. Sunyach, Comptes Rendus de l'Académie des Sciences—Series IIB (Fluids Mechanics) 328 (2000) 749.
[12] M. Amitay, A. Glezer, International Journal of Heat and Fluid Flow 23 (2002) 690.
[13] J. Tensi, I. Boué, F. Paillé, G. Dury, Journal of Visualization 5 (2002) 37.
[14] Y. Yassour, J. Stricker, M. Wolfshtein, Proc. eighth Int. Heat Transfer Conference, San Francisco, USA, 1183 (1986).
[15] A. Glezer, M.G. Allen, Synthetic Jet Actuators for cooling heated bodies and environments, US Patent No. 6123145 (2000).
[16] A. Glezer, J. Vukasinovic, Bulletin of the American physical society, Division of Fluid Dynamics 45 (2000) 136.
[17] H. Martin, Advances in Heat Transfer 13 (1977) 1.
[18] S.V. Garimella, Annual Review of Heat Transfer XI (2000) 413.
[19] Y. Kokoshima, A. Shimizu, T. Murao, Proc. third triennial Int. Symp. Fluid Control, Measurement, and Visualization FLUCOME'91, ASME, San Francisco, 205 (1991).
[20] H. Maki, A. Yabe, Proc. Heat Transfer in Convective Flows HTD-107, Philadelphia, Pennsylvania, 163 (1989).
[21] V. Tesař, M. Jílek, Z. Randa, Proc. Topical Problems of Fluid Mechanics 2001, Prague, 121 (2001).
[22] V. Tesař, M. Jílek, Z. Randa, Proc. Colloquium Fluid Dynamics 2001, Prague (2001).
[23] V. Tesař, M. Jílek, Z. Randa, MECH 006-Workshop 2002, Czech Technical University, Prague (2002).
[24] C. Herman, Annual Review of Heat Transfer 11 (2000) 495.

[25] R.J. Goldstein, H.H. Cho, Experimental Thermal and Fluid Science 10 (1995) 416.
[26] S.J. Kline, F.A. McClintock, Mechanical Engineering 75 (1953) 3.
[27] J. Lepičovský, K.K. Ahuja, R.H. Salikuddin, Journal of Propulsion and Power 2 (1986) 149.
[28] Z. Trávníček, F. Křížek, Heat and Mass Transfer 35 (1999) 351.